JEE Journal of Ecological Engineering

Journal of Ecological Engineering, 2025, 26(2), 85–100
https://doi.org/10.12911/22998993/195974
ISSN 2299–8993, License CC-BY 4.0

Received: 2024.11.07
Accepted: 2024.12.15
Published: 2025.01.01

Numerical and experimental study of the impact of biofuel generated from waste olive oil on performance and emissions of IC engines

Munaf D. F. Al-Aseebee[1, 2*], Ahmed Ketata[2, 3], Husam Abdul Rasool Hasan[4], Olfa Moussa[2], Zied Driss[2], Mohamed Salah Abid[2], Ahmed Samir Naje[1], Tholfekar Habeeb Hussain[1]

[1] College of Engineering, AL-Qasim Green University, Babylon 51031, Iraq
[2] Laboratory of Electromechanical Systems, National School of Engineers of Sfax), University of Sfax, B.P. 1173, Road Soukra km 3.5, 3038 Sfax, Tunisia
[3] Preparatory Institute for Engineering Studies of Gabes, University of Gabes, Tunisia
[4] Ministry of Higher Education & Scientific Research, Department of Studies, Planning & Follow-up, Baghdad, 10011, Iraq
* Corresponding author e-mails: manafal_asseby@wrec.uoqasim.edu.iq

ABSTRACT

As a substitute for conventional fossil fuels, biodiesel may be a potential future choice to deal with the scarcity of fossil fuels while lowering the emissions of pollutants from internal combustion engines. The aim of this research is to assess, through experiments and statistical analysis, the effects of using a diesel-biofuel blend on the performance and emissions of a single-cylinder direct injection engine. Utilizing used oil derived from trees of olive in the Tunisian region of Sfax was presented in this scientific study. As for the producer of biofuels from recycled olive oil, a chemical esterification procedure was carried out. Six mixes with varying amounts of diesel and biofuel were created and tested at the test facility for single-cylinder engines. The experimental results were compared to a one-dimensional engine model in terms of torque and exhaust emissions, and the results showed a good agreement between the test and the numerical data. For a better understanding of the elements that affect the engine's response to changes in fuel composition, the thermodynamic parameters of the engine for each formulation have also been presented. According to the investigation, a blend of 80% pure diesel and 20% methyl ester-based oleic acid-based biofuel would be a workable fuel option for cleaner exhaust emissions while providing essentially the same performance.

Keywords: fossil diesel, OAME biofuel, transesterification reaction, waste olive oil, IC engines, pollutant emissions.

INTRODUCTION

In recent years, many initiatives have been taken to improve the performance and emissions of internal combustion engines (ICEs) by using alternative fuels [1–2], downsizing [3], and turbocharging [4–5]. Most of the world's energy is generated by fossil fuels, which has led to an increase in air pollution. The main cause is the exhaust emissions generated by the combustion of fossil fuels, especially carbon dioxide (CO_2), nitrogen dioxide (NO_x), and sulfur dioxide (SO_x) [6–7]. In order to address these environmental issues, it is now more important than ever to research clean fuel alternatives to fossil fuels. Bio combustible materials are fuels made from non-fossil and renewable organic resources. They belong to two main families: biofuels and vegetable oils are alternatives to diesel fuel, while bioethanol, butane, and methanol are gasoline alternatives [1–8]. Some of the advantages of biofuels are their availability, non-toxicity, renewability, and biodegradability [9–10]. Vegetable and animal fats can be used to create a biofuel, an ecological biofuel that is renewable. It helps reduce engine pollution emissions and can be used straight to feed the engine [11–12]. Triacetin, which was introduced as an additive for spark-ignition gasoline engines, was made by Dewal [13] formality utilizing the leftover glycerol from the biodiesel production process. It was demonstrated that a considerable decrease in the tested engine's emissions occurred upon the application of 4.31% triacetin. Pure Vegetable Oil (PVO) has been demonstrated to directly cause combustion issues in internal combustion engines [14–15]. The main drawbacks of using PVO directly, according to de Oliveira Camargo [16], are connected to its low volatility and high viscosity at room temperature, which might result in the buildup of carbon deposits in engine parts. Shrigiri [17] It is made clear that using the PVO continuously leaves large carbon deposits on the noses of injectors, cylinder heads, valves, and piston heads. The reason for these deposits is poor injection spray. The most significant technique for enhancing the properties of plant-based oils, animal fats, and culinary waste by turning them into biofuel is transesterification. According to a number of research, alcoholic vegetable oils can be changed into an ester that is similar to diesel fuel by using an alkaline catalyst to change their physicochemical composition [18, 19]. In order to optimize the input power, reaction time, oil-to-methanol molar ratio, turntable speed, and fan cooling speed for the trans esterification of cottonseed oil into biodiesel, Kumar and Pal [20] created a novel approach based on a home microwave oven. 99.5% of the amount produced by a conventional magnetic stirrer in terms of cottonseed biodiesel output. Experimental research on the properties of biofuel made from combining rapeseed and soybean oils was conducted by Li [19]. They looked at how much catalyst was used, how long the reaction took to happen, and how much alcohol there was in relation to the oils. The mole ratio of the methanol oil, which was 5:1, allowed them to deduce that the best reaction conditions were achieved at a reaction temperature of 55 °C. The physicochemical characteristics of a biofuel made from Karanja oil were assessed by Karikalan and Chandrasekaran [21] and contrasted with ASTM (American Society For Testing and Materials) standards. In comparison to pure vegetable oil, they observed a modest improvement in the calorific value. On the other hand, the enhancement of other properties including viscosity, density, and volatility is a highly noteworthy benefit of the oil's esterification. The physicochemical characterization and thermal behavior of the biofuel made from crude Moringa seed oil and its mixtures with the diesel were ascertained by Aroua [22], and Al-Aseebee [23]. The study found that the global fuel properties improved in comparison to the oil properties, which showed a 4.675 $mm^2 \cdot s^{-1}$ reduction in kinematic viscosity at 40 °C. The biofuel density is significantly lower at 876.2 $kg \cdot m^{-3}$ than the oil density of 892.8 $kg \cdot m^{-3}$. The performance and emissions of a single-cylinder direct injection 4-stroke diesel engine powered by diesel fuel mixes containing the methyl and ethyl esters of Karanja vegetable oil were examined by Naik [24]. Dynamic injection behaviors on contemporary common-rail injection systems running with high and low proportion blends of biofuels were studied by Hou and Zhang [25]. They came to the conclusion that for low-proportioned biofuel blends, the mean volume quantity of injection rises by a percentage ranging from 36% to 43%. The tribological interaction between motor oil and biofuel soot was investigated by Li and Zhang [26]. The potential of the biofuel soot to repair friction surfaces and build a protective layer was demonstrated, which improved the biofuel soot's anti-wear properties. However, Chourasia and Lakdawala [27] demonstrated that biofuels of extremely corrosive nature can harm the engine's injection components, which is a serious problem. Fu [28] investigated how adding an n-butanol additive affected the typical rail injector spray characteristics of contemporary diesel engines. According to reports, pure biofuel exhibits far larger spray tip penetration and spray cone angle than blends with additives based on n-butanol. El Morsi [29] used three blends of conventional diesel and waste olive oil biofuel to experimentally study the exhaust emissions and engine performance at various engine loads. They observed that the engine's exhaust emissions improved when the waste olive oil biofuel was carefully blended. On the other hand, compared to diesel, biofuel and its blends have higher NO_x emissions, specific fuel consumption, and thermal efficiency. Eucalyptus biofuel was investigated by Tarabet and Loubar [30] as a potential alternative fuel for direct ignition engines. According to their results, the specific fuel consumption of eucalyptus biofuel is slightly higher than that of diesel. Waste oil causes many ecological problems such as river water pollution [31]. It has great potential as a biofuel due to its high content of triglycerides and free fatty acids. The present work investigates the potential use of oleic acid methyl ester (OAME) extracted from waste olive oil as an alternative biofuel through extensive experimental and computational studies.

OLEIC ACID METHYL ESTER BIOFUEL

Manufacturing

Figure 1 illustrates the different stages that the synthesis of methyl oleate in this study went through. First, waste oil made from leftover olive oil was weighed using a balance as shown in Figure 2a. The basic catalytic components, potassium hydroxide with the chemical formula KOH and methanol with the chemical formula CH_3OH, were combined before adding them to the reaction vessel for the transesterification reaction. The transesterification reaction, as shown in Figure 1b, was then started by adding a mixture of methanol and potassium hydroxide. Vegetable oils can be converted into biofuels through transesterification reactions. The reaction temperature, the molar ratio of alcohol to oil, the catalyst, and the type of alcohol are the three main parameters that affect the efficiency of the reaction. In this work, the basic catalysis occurred at a reaction temperature of 60 °C with a molar ratio of methanol to olive oil of 6:1. Figures 2b and 2c illustrate the use of a three-necked piston reactor with a

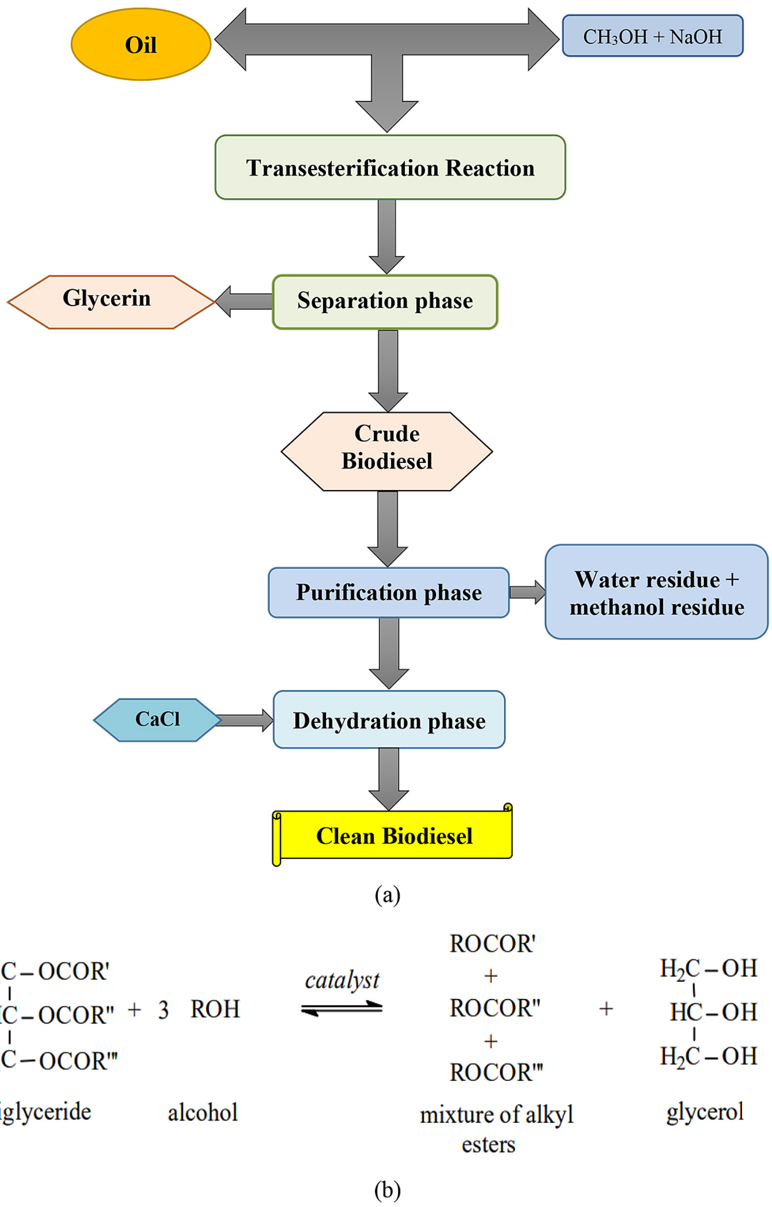

Figure 1. (a) OAME biodiesel production flow chart and (b) transesterification reaction.

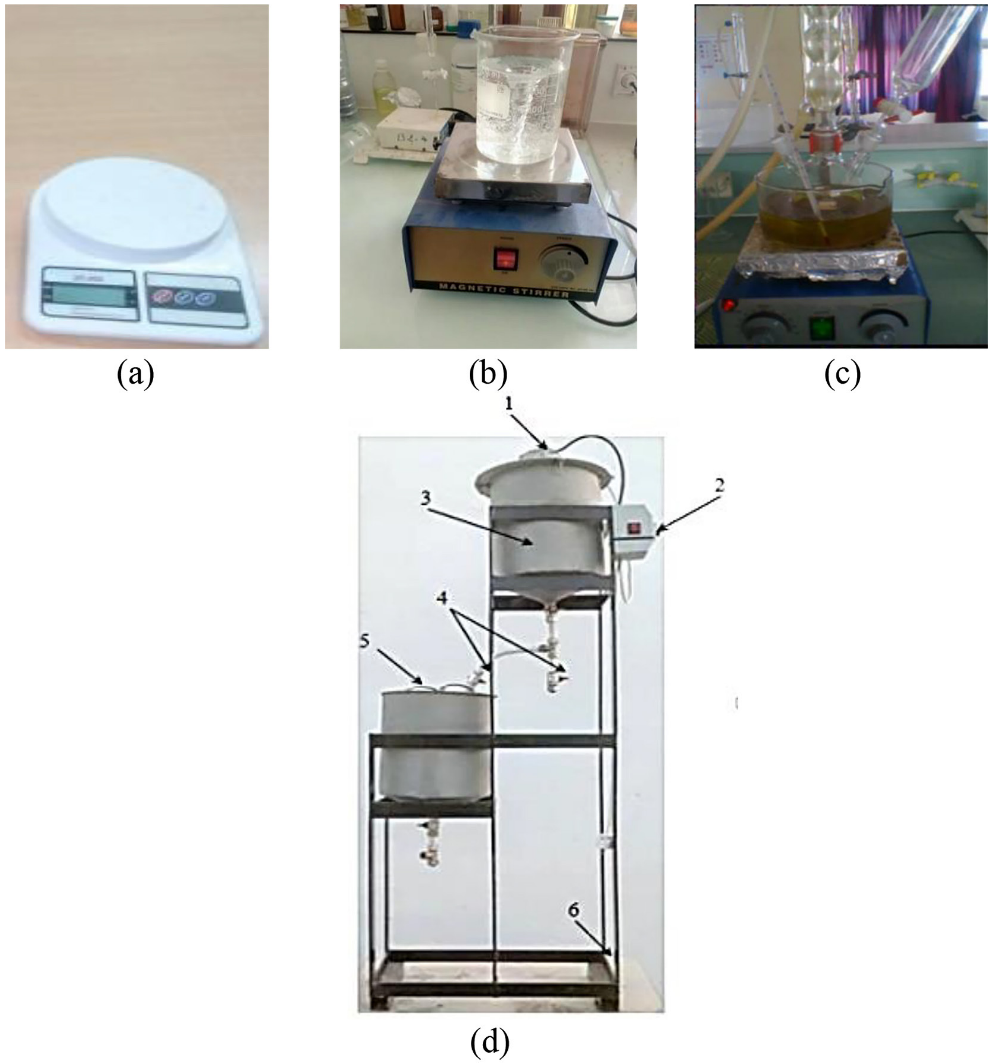

Figure 2. (a) Balance, views of (b) CH_3OH and KOH mixture, and (c) transesterification reaction operation, and (d) biodiesel production pilot plant: 1 – agitation system, 2 – electric controller, 3 – esterification reactor, 4 – valves, 5 – separation tank, 6 – metal support

reflux condenser and a thermometer as a laboratory instrument for the transesterification reaction to measure the reaction temperature. The combination of reaction components was heated to the proper temperature using a magnetic stirrer with a hot plate and a temperature controller and a paraffin oil bath to achieve the desired temperature. To produce large quantities of biofuel, a large plant was built, as shown in Figure 2d. The laboratory scale is not sufficient to produce large quantities of biofuel. The same steps as for the laboratory scale technique were followed. The plant to produce the biofuel consisted of a 10 L esterification reactor equipped with a stirrer system and heating resistors to raise the temperature to 100 °C. There was also a 15 L sedimentation tank for the separation of crude methyl oleate and glycerol. To obtain a pure phase of biofuel, the crude methyl oleate was filtered from the separation process and dehydrated by adding calcium chloride ($CaCl_2$). The net biofuel was stored for the final physicochemical characterization stage before being used as a feedstock for internal combustion engines.

Physical and chemical analysis

Tests and comparisons between the produced oleic acid methyl ester's properties in a mixture and as pure with the petroleum-based diesel were conducted. The National School of Engineers in Sfax has measured the density, kinematic viscosity, refraction index, and saponification. Based on the tests, Table 1 shows the kinematic and dynamic viscosities of the used olive oil as well as the methyl ester that was created at 40 °C. Based on these findings, it is evident that the transesterification reaction played a major role in the end product's kinematic viscosity being reduced from 62.48 $mm^2 \cdot s^{-1}$ to 4.32 $mm^2 \cdot s^{-1}$. Comparing the measured kinematic viscosity of the net oleic acid methyl ester to the European EN14214 (European Standard) and the American ASTM standards, as shown in Table 1, reveals that it is well within a range appropriate for engine operation. Furthermore, because the transesterification reaction reduced the observed density of the oleic acid methyl ester from 0.926 to 0.898 $kg \cdot l^{-1}$, it satisfies standard standards. Similarly, the average acid value for the oleic acid methyl ester has dropped from 0.6 mg $KOH \cdot g^{-1}$ for the used olive oil to 0.4 mg $KOH \cdot g^{-1}$.

Table 1. Comparing the physicochemical parameters of OAME and used olive oil to ASTM and EN14214 standards

Property	Olive Oil	OAME	EN14214	ASTM
Refraction index	1.47	1.452	–	–
Saponification value, mg KOH·g	196.5	–	–	–
Cetane index	–	52	51 min	47 min
Acid value, mg KOH·g	0.63	0.4	0.5 max	0.5 max
Lodine value, g I_2·100 g	123	110	120 max	–
Density at 40 °C, kg/l	0.926	0.898	0.86–0.9	0.88
Kinematic viscosity at 40 °C, $mm^2 \cdot s$	62.48	4.32	3.5–5	1.9–6
Flash point, °C	312	162	120 min	101 min
Lower Calorific value, kJ/kg	–	40890	–	35000

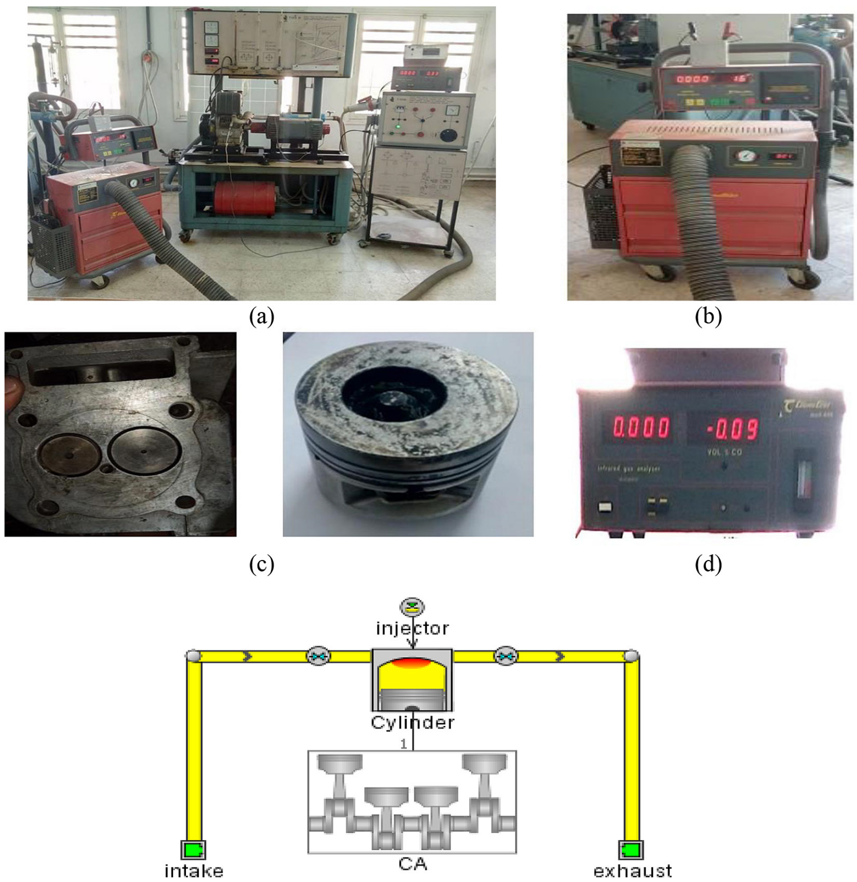

Figure 3. Views of (a) Experimental setup, (b) emission gas analyzer (c) engine piston and head valves, (d) emission gas analyzer control panel and (e) 1D engine numerical model

ENGINE EXPERIMENT COMPETENCE

As illustrated in Figure 3, the engine test rig consists of a single-cylinder, four-stroke diesel internal combustion engine with a crankshaft connected to an eddy current dynamometer, an exhaust gas emission analyzer, an exhaust manifold thermocouple installed for temperature measurement, and a fuel consumption quantification system fixed at the top dashboard. The engine under test is called the 15 LD (Lombardini Diesel Engine). It has a 0.315 L overall displacement and is air-cooled, direct-injected, and naturally aspirated. It has a 20.3:1 compression ratio. The engine cylinder has a 78 mm bore and a 66 mm stroke. As seen in Figure 3b, the engine's piston head contains a hemispherical cavity known as the bowl that is 5 mm offset from the cylinder's center. Engine tests for a range of engine rotational rates, from 800 rpm to 4000 rpm, were conducted for this study. A constant injection rate and load were applied to the engine to set its rotational speed. By employing the brake dynamometer to break the crankshaft, the engine load was adjusted, and the engine's rotational speed was kept at each test point. The engine brake power was calculated with the generated electrical power P_e in the dynamometer considering its mechanical efficiency as follows:

$$P_b = \frac{P_e}{n_m} \tag{1}$$

The BSFC has been computed as follows, with a unit of $g \cdot kWh^{-1}$:

$$BSFC = 3.6\ 10^6 \frac{r}{P_b} \tag{2}$$

where: r is the fuel consumption in grams per second and P_b is the brake power in Watt.

The engine was initially fed with pure Diesel, matching the B 0% case under consideration, for each tested rotational speed. This allowed for the measurement of the engine's output brake torque as well as its emissions of NO_x, CO, and CO_2. Next, using the fuel control panel to match the other fuel blend cases under investigation, the volumetric fraction of pure Diesel is gradually raised while the volumetric fraction of the generated oleic acid methyl ester is gradually increased from B20% (blend from biodiesel fuel 20% and fossil diesel fuel 80%) to B 100%.

ONE-DIMENSIONAL COMPUTATIONAL METHODOLOGY

In this work, the tested engine running on pure diesel or several explored blends ranging from B0% (fossil diesel fuel 100%) to B100% (100% Pure Biodiesel) was simulated using a gas dynamics solver based on a staggered grid finite-volume discretization method. An overview of the tested engine's comparable 1D model is shown in Figure 3e. It is made up of several versions of crankshafts, cylinders, intake and exhaust valves, and ducts. The other engine components are based on analytical models in which they are modeled as boundary conditions, while the ducts' model is based on the numerical finite volume approach. The reader may consult our earlier works that have been published for additional information regarding the engine simulation model [32–34]. The implicit formulation's solutions to the flow conservation equations for the ducts model are enthalpy, momentum, and continuity, as indicated below:

$$\frac{\partial m}{\partial t} = \sum_{boundaries} \dot{m} \tag{3}$$

$$\frac{\partial \dot{m}}{\partial t} = \frac{dpA + \sum_{boundaries}(\dot{m}u) - 4C_f \frac{\rho u|u| dxA}{2D} - \frac{1}{2}k_p \rho u|u|A}{dx} \tag{4}$$

$$\frac{\partial(\rho H u)}{\partial t} = \sum_{boundaries} \dot{m}H + u\frac{dp}{dt} - hA(T_f - T_w) \tag{5}$$

where: $\dot{m}$ is the mass flow rate, ρ is density, u is velocity, H is the total enthalpy and t is time. p is static pressure, T_f is the fluid static temperature, T_W is the wall temperature, C_f is the Fanning friction coefficient, k_p is the pressure loss coefficient, and h is the heat transfer coefficient. A is the pipe section of any cross-sectional shape and D its equivalent hydraulic diameter. The volume of the whole system was discretized into many volumes. Each discretized volume denotes each flow split, and the individual pipe is separated into single or several volumes. Each of which represents a split in the flow.

The following formula was used to estimate the fuel injector's delivery mass flow rate:

$$\dot{m}_{inj} = \frac{6\ \eta_V \rho_{ref} N V_d R_{AF}}{n_c\, p_w} \tag{6}$$

where: η_v is the volumetric efficiency of the injector, ρ_{ref} is a reference density equal to

1.16 kg·m^{-3}, N is the engine speed given in rpm, V_d is the engine displacement, R_{AF} is the fuel-to-air ratio specified from the experimental study, p_w is the injector pulse width given in crankshaft angle degrees, and n_c is the number of cylinders. The engine cylinder's heat transport was modeled using the well-known Woschni's model. the heat transfer coefficient h_c can be calculated as follows:

$$h_c = \frac{K_1 p^{0.8} u^{0.8}}{B^{0.2} T^{K_2}} \tag{7}$$

where: B is the cylinder bore, C_1 and K_2 are constants of the model equal to 3.014 and 0.5 respectively, p is the in-cylinder pressure, T is the in-cylinder temperature, and u is the average cylinder gas velocity.

The average cylinder gas velocity u is calculated as follows:

$$u = C_1 u_p + C_2 \frac{V_d T_r}{p_r V_r}(p - p_m) \tag{8}$$

where: u_p is the mean piston speed, C_1 and C_2 are constants of the model, V_d is the displacement volume, V_r is the working fluid volume prior to combustion, p_r is the working fluid pressure prior to combustion, T_r is the working fluid temperature prior to combustion, and p_m is the motoring fluid pressure at the same crankshaft angle as the fluid pressure p. Additionally, where C_1 and C_2 are the constants of the model.

An empirically developed model that asserts that total engine friction is a function of peak cylinder pressure, mean piston speed, and mean piston squared speed was used to estimate the engine's mean effective friction pressure, or FMEP. The FMEP is provided in this manner:

$$\begin{aligned} FMEP = {} & c_f + c_{f,p}\, p_{max} + \\ & + c_{f,u1}\, u_p + c_{f,u2}\, u_p^2 \end{aligned} \tag{9}$$

where: c_f is a constant, $c_{f,p}$ is the coefficient of the cylinder maximum pressure p_{max}, $c_{f,u1}$ and $c_{f,u2}$ are the first and second order coefficients of the mean piston speed u_p.

The burn rate for direct-injection compression-ignition engines was calculated based on the three-term Wiebe function coming from the superposition of the three normal Wiebe curves. These Wiebe curves approximate the typical shape of a direct injection (DI) compression ignition. The purpose of using three functions is to make it possible to model the premixed and diffusion portions of the combustion process. Based on this model, the cumulative burn rate was calculated as follows:

$$BR(\theta) = \eta_c \left(\begin{matrix} F_p\left[1 - e^{-W_{cp}(\theta - S_{oi} - I_d)^{E_p+1}}\right] + \\ + F_m\left[1 - e^{-W_{cm}(\theta - S_{oi} - I_d)^{E_m+1}}\right] + F_t\left[1 - e^{-W_{ct}(\theta - S_{oi} - I_d)^{E_t+1}}\right] \end{matrix} \right) \tag{10}$$

where: η_c is the combustion efficiency, θ is the crankshaft angle, I_d is the ignition delay, S_{oi} is the start of the ignition angle, E_p, E_m, and E_t are the Wiebe premix, main and tail exponents respectively, W_{cp}, W_{cm}, and W_{ct} are the Wiebe premix, main and tail constants respectively, F_p, F_m, and F_t are the Wiebe premix, main and tail fractions respectively.

The main Wiebe fraction F_m is calculated as follows:

$$F_m = 1 - F_p - F_t \tag{11}$$

The Wiebe premix, main and tail constants were calculated as follows:

$$W_{cp} = \left(\frac{D_p}{2.302^{1/E_p+1} + -0.105^{1/E_p+1}}\right)^{-(E_p+1)} \tag{12}$$

$$W_{cm} = \left(\frac{D_m}{2.302^{1/E_m+1} + -0.105^{1/E_m+1}}\right)^{-(E_m+1)} \tag{13}$$

$$W_{ct} = \left(\frac{D_t}{2.302^{1/E_t+1} + -0.105^{1/E_t+1}}\right)^{-(E_t+1)} \tag{14}$$

where: D_p, D_m, and D_t are the Wiebe premix, main and tail durations respectively.

RESULTS AND DISCUSSION

Brake torque

The brake torque distribution of the engine under test with various fuel blends is superposed in Figure 4a. These findings show that there is a good agreement between the experimental and numerical results. As the concentration of oleic acid methyl ester biofuel rises, the brake torque falls. When comparing low and medium engine rotational rates (800 rpm to 2500 rpm) to high engine speeds (2500 rpm to 3500 rpm), the brake torque decline is much greater.

The engine reaches its maximum braking torque around 1400 revolutions per minute. As an example, with the B 60% blend, the peak torque is reported to have fallen by 33%, but the average percentage decrease in brake torque is observed to be 41%. Furthermore, as small variations in brake torque throughout the whole speed range have been observed with low biofuel percentages, the results demonstrated that the brake torque is overly

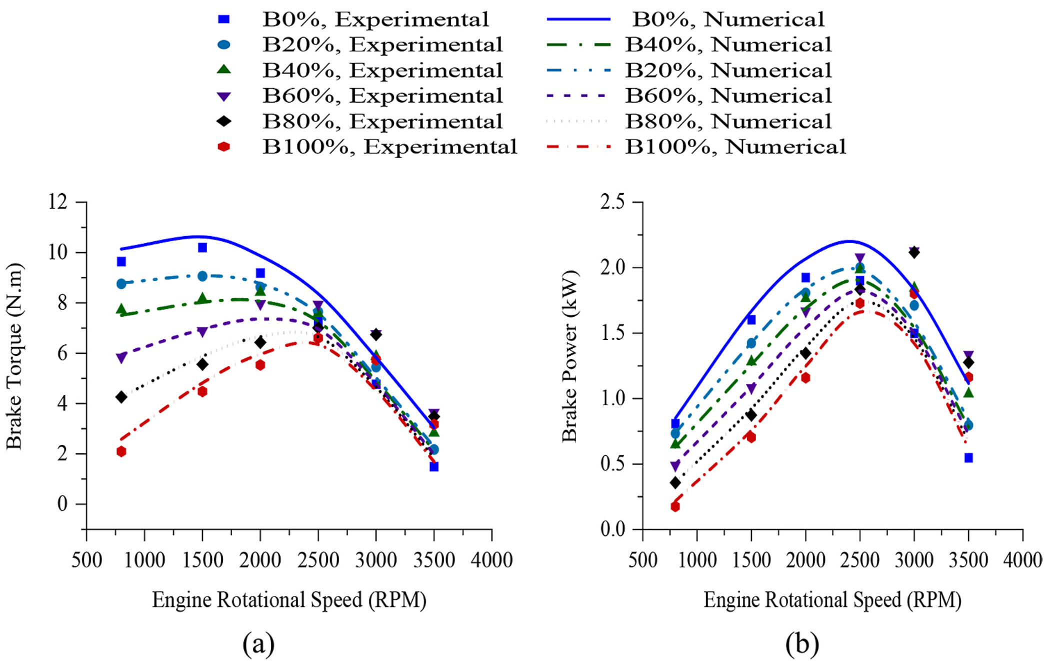

Figure 4. Cycle-average brake (a) torque and (b) power for the considered diesel-OAME blends

sensitive to the biofuel concentration in the mix. Low fuel calorific value as the amount of biofuel is increased in the blend can be the reason for the observed decrease in brake torque at low and medium rotational speeds of the engine, even though combustion with high concentrations of biofuel is better than that of pure diesel because the biofuel addition will lead to a high oxygen concentration of the blend. In comparison to pure diesel, the addition of biofuel to the blend causes the mixture to have a higher density, low volatility, and high viscosity, which slows down combustion [35].

Brake power

The variation in the tested engine's brake power with respect to rotational speed for the several diesel-biofuel mixes under investigation is shown in Figure 4b. These findings prove a good agreement between the numerical and experimental results, supporting the validity of the computational approach. Since the brake power depends on both the rotational speed and the brake torque, observations akin to those regarding the brake torque have also been made. The brake power dramatically drops as the blend's oleic methyl acid ester percentage rises. At the highest power point, the brake power loss is less significant, but as engine speeds increase and fall, it becomes increasingly significant. For example, at a rotational speed of 1500 rpm, an average percentage loss of 37.5% in braking power and a peak percentage decrease of 16.33% in brake torque have been observed for the B 60% scenario in comparison to the pure diesel case. Additionally, as the proportion of oleic acid methyl ester biofuel in the mix grows, there has been a modest shift in the brake power peak point towards the engine's low rotational speeds. For instance, in the pure diesel and B 100% situations, the maximal brake power happens at a rotational speed of 2384 rpm and 2634 rpm, respectively. As a result, the point of optimal braking power is moved towards higher rotational speeds the more biofuel there is in the mixture.

Consumption of fuel

The variation in the tested engine's brake-specific fuel consumption (BSFC) with respect to rotational speed for the several diesel-biofuel blends under investigation is shown in Figure 5a.

These findings prove a strong agreement between the numerical and experimental results, supporting the validity of the numerical approach. Additionally, it has been proved that all gasoline mixes under investigation have minimal fuel consumption at medium engine rotational speeds, which corresponds to the greatest brake power levels. Except for pure diesel fuel, the BSFC steadily rises outside of this medium speed range, which spans from 2000 rpm to 3000 rpm. It achieves its highest value at the lowest engine rotational speed in the

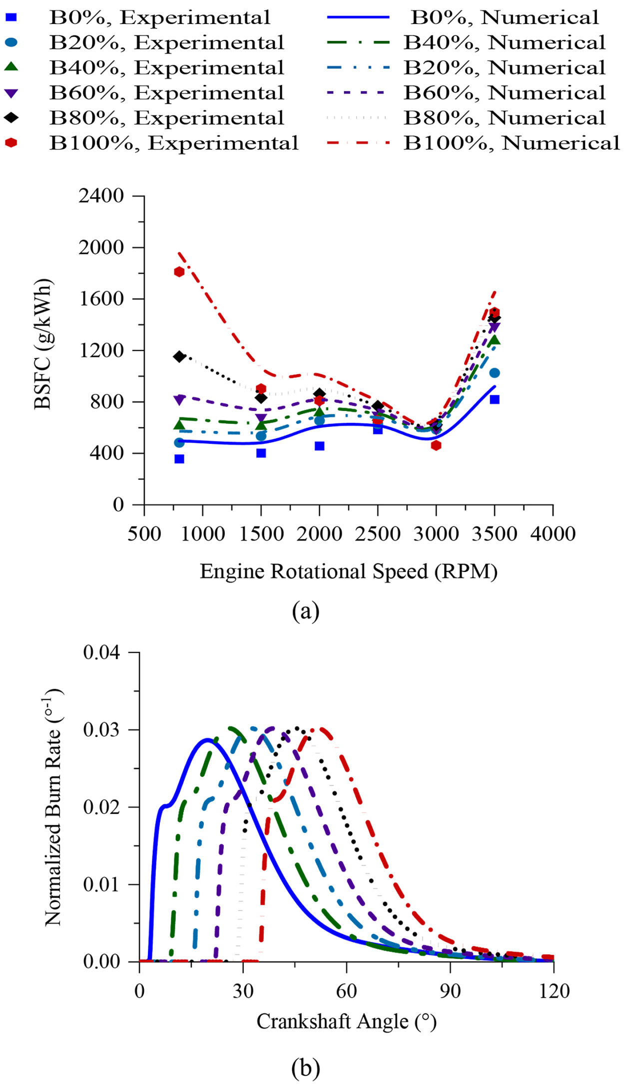

Figure 5. Cycle-average (a) brake specific fuel consumption and (b) normalized burn rate for the considered diesel-OAME blends.

middle regime. Furthermore, the amount of gasoline consumed is extremely dependent on the oleic acid methyl ester biofuel's content. For example, because the engine is running only on diesel, the BSFC is 472 g·kWh^{-1} during idle. As more oleic acid methyl ester biodiesel is added to the mixture, the BSFC grows steadily. As a result, the maximum value of 1920 g·kWh^{-1} is recorded with the B 100% case at an engine rotation speed of 800 rpm. This results from the earlier finding that biofuel has a lower fuel calorific value than pure diesel, which limits its capacity to produce electricity.

Rate of burn

The instantaneous change in the burn rate, normalized to the total fuel mass, with respect to the crankshaft angle at an engine rotation speed of 800 rpm is displayed in Figure 5b. As the concentration of oleic acid methyl ester biofuel increased, Figure 5b's results showed a modest rise in the in-cylinder combustion's burn rate. For instance, when the fuel composition is altered from the B 0% case to the B 100% case, the normalized burn rate rises by 5.58%. The anticipated outcome is that the oleic acid methyl ester biofuel has a higher combustion completeness than pure diesel due to its increased oxygen molecule content. Furthermore, research has demonstrated that when the final blend's oleic acid methyl ester biofuel content increases, the start of combustion delays. For example, in the B 100% and B 0% situations, the combustion begins at crankshaft angles of 35° and 1.9° after the top dead center (TDC), respectively. The engine brake torque and, consequently, the brake power output are significantly reduced as a result of this combustion delay. This is easily inferred from the fact that the cylinder will only partially recover the potential combustion force operating on it since the combustion will not begin at the necessary moment or the TDC point. Thus, it can be concluded that delayed combustion rather than high combustion incompleteness is the primary cause of the engine's drop in braking power observed in the event of a growing concentration of oleic acid biofuel methyl ester.

PV diagram of thermodynamics

The thermodynamic instantaneous characteristic of the engine in terms of its pressure-volume (PV) has been presented in Figure 6 to help further understand the factors behind the low-generated power of the oleic acid methyl ester biofuel in addition to the previously described delay in burning. It is important to note that the capacity has been adjusted to match the bottom dead center (BDC) maximum cylinder volume.

These findings indicate that the power stroke section of the engine PV diagram, for the four rotational speeds ranging from 800 rpm to 3500 rpm, is highly sensitive to variations in the blend's oleic acid methyl ester biofuel concentration. Recall that the engine PV diagram's power stroke section corresponds to the area where the exhaust valve starts to open as the pressure decreases from its greatest value to the atmospheric value. However, at low engine speeds, this shift in the power stroke section of the PV diagram with the fuel mixture is more noticeable. Thus, the pressure decreases with a high slope in the B 0% case because the engine is running on pure diesel, but it decreases with a weak slope in the B 100% scenario. The observed variation in the kinematic viscosity between the blends – where a higher viscosity is obtained when biofuel is added – could be the cause of this. As a result, the combustion chamber's gas will behave differently when it expands suddenly. Since the engine work is directly related to the integral of the in-cylinder pressure relative the cylinder capacity, these facts may help to explain the decline in power as the proportion of biofuel in the blend increases.

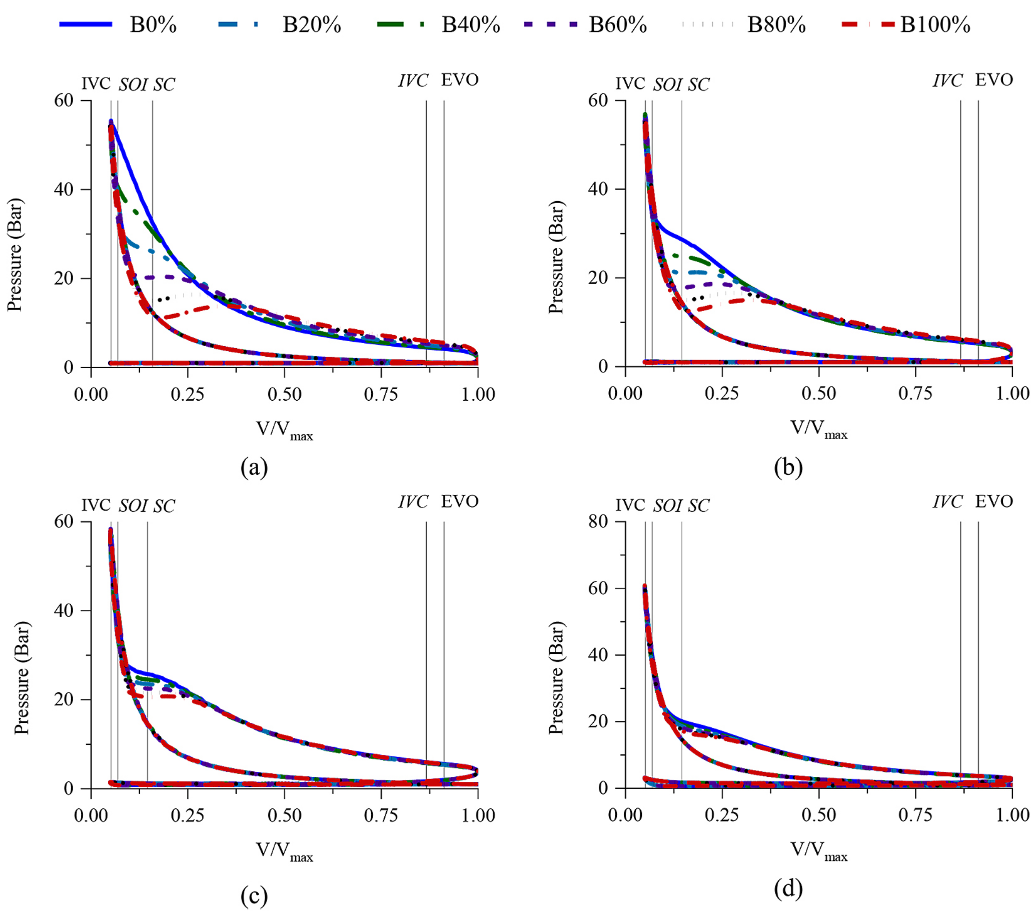

Figure 6. Effect of diesel-OAME blend on pressure-volume diagram under engine rotational speeds of (a) 800 rpm, (b) 1500 rpm, (c) 2500 rpm and (d) 3500 rpm

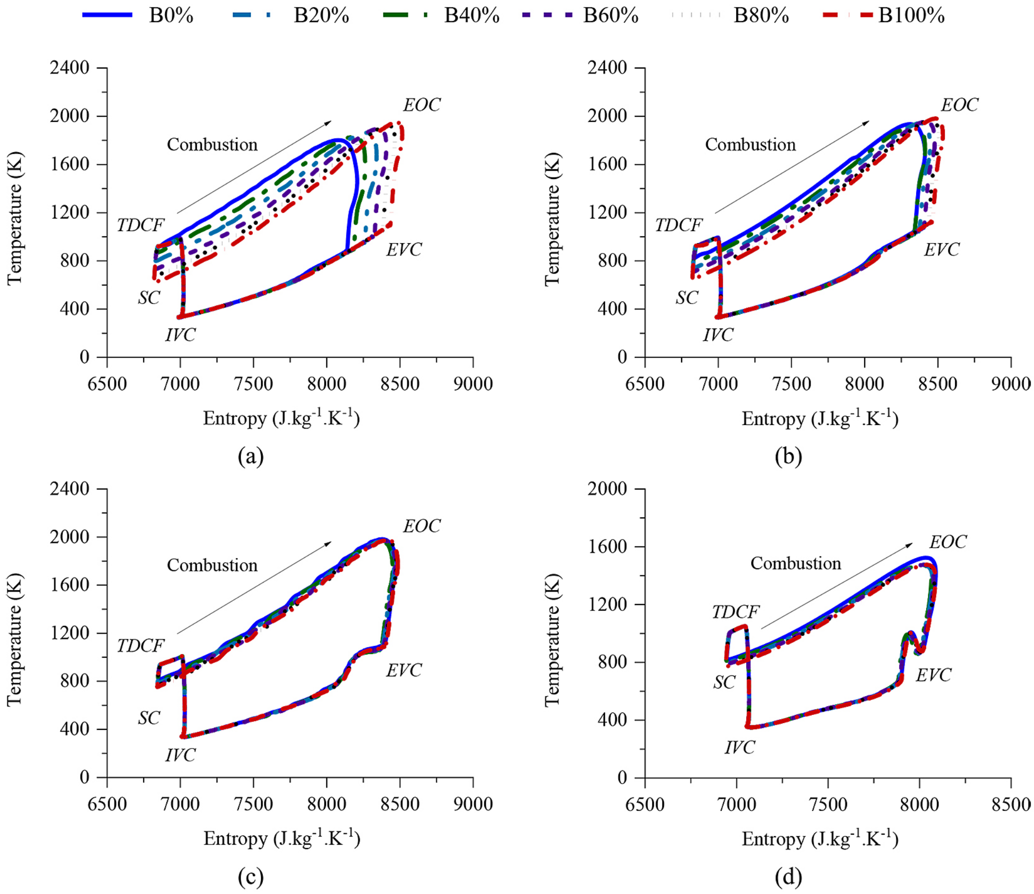

Figure 7. Effect of diesel-OAME blend on temperature-entropy diagram under engine rotational speeds of (a) 800 rpm, (b) 1500 rpm, (c) 2500 rpm and (d) 3500 rpm

TS diagram of thermodynamics

The temperature-entropy diagram for the six cases under investigation and four rotational speeds ranging from 800 rpm to 3500 rpm are displayed in Figure 7. The enthalpy exchange that occurs during the cycle and the generation of loss are both reflected in the temperature-entropy diagram. These findings demonstrate that a larger heat release during combustion arises from increasing the quantity of oleic acid methyl ester biofuel in the blend, since high-temperature fluctuations are shown in the temperature-entropy diagram for all rotational speeds.

For example, the in-cylinder temperature for the B 100% and B 0% cases is 1965 K and 1806 K, respectively, at a rotational speed of 800 rpm at the end of combustion (EOC), but the temperature immediately following the commencement of combustion is almost identical at 918 K. Since identical TS (temperature entropy) diagrams have been observed under rotational speeds higher than 2500 K, it is determined that this difference in heat release during combustion is more significant at low rotational speeds. The results of the burn rate in the previous section, which show that its effect is more pronounced at low rotational frequencies, can be used to explain this fact. Furthermore, when the percentage of biofuel in the blend increases, the change in entropy also increases dramatically. As a result of using a higher percentage of blended biofuel, the engine loses heat more quickly. Thus, at an engine rotation speed of 800 rpm, the specific entropy change during the cycle's combustion is 1298 $J \cdot kg^{-1} \cdot K^{-1}$ when the engine is fueled by pure diesel and increases to 1634 $J \cdot kg^{-1} \cdot K^{-1}$ when the engine is fueled by pure biofuel, representing a total increase in the entropy change of approximately 26%. Thus, the engine heat loss is not affected by the amount of biofuel in the blend at high rotational speeds above 2500 rpm, when the difference in entropy change is insignificant.

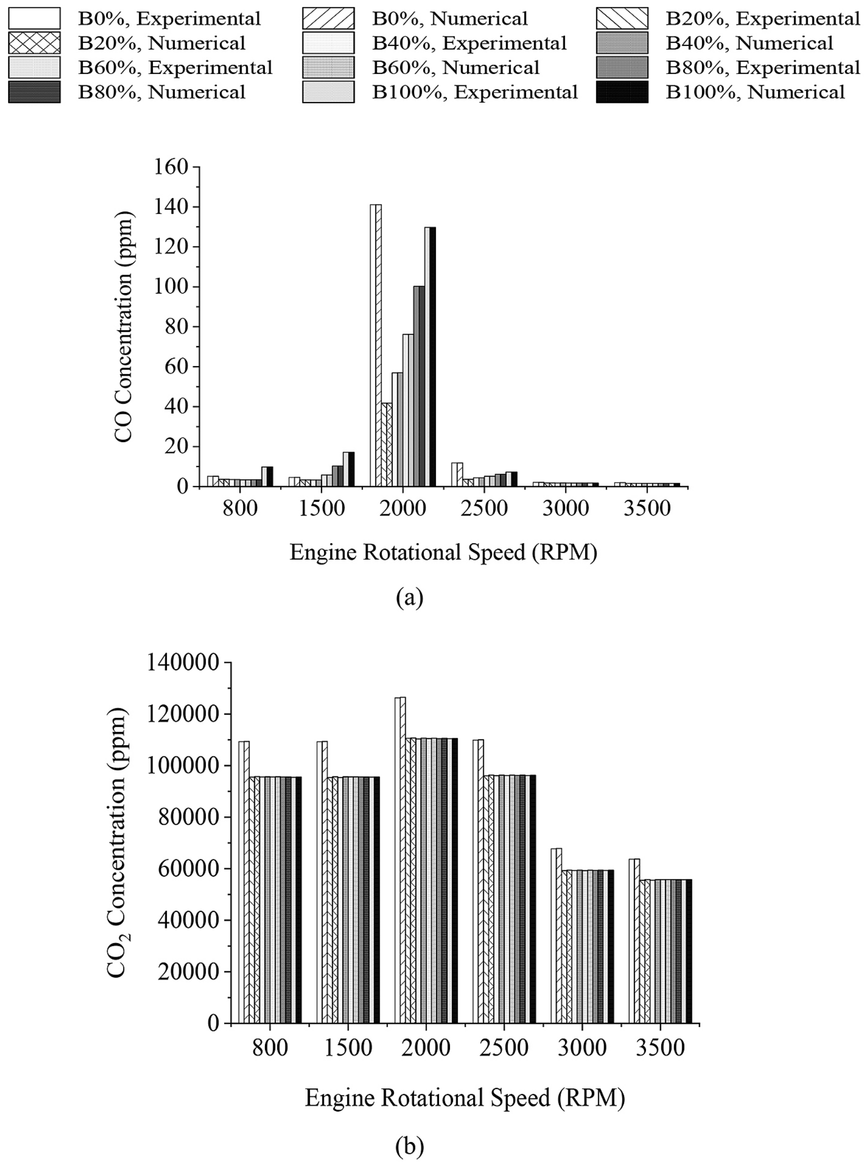

Figure 8. Effect of diesel-OAME blend on cycle average (a) CO and (b) CO_2 emissions

Carbon monoxide release

Figure 8a shows the experimental and numerical expected cycle averages of carbon monoxide (CO) in the exhaust of the test engine, expressed in parts per million (ppm), for the various fuel blends studied, over the speed range of 800 rpm to 3500 rpm. These results show strong agreement between the experimental and numerical results. CO emissions increase significantly when the speed decreases from 3500 to 2000 rpm. CO emissions peak at 2000 rpm, a speed characteristic of high output torque, and then gradually decrease to 800 rpm as the speed decreases. The results show that the addition of up to 20% methyl oleate biofuel by volume significantly reduces CO emissions, with 20% having the lowest CO emissions. When the volume fraction of biofuel exceeds 20%, CO emissions increase, but remain below the levels observed when the engine is operated on pure diesel. For example, at 2000 rpm, CO emissions for Cases B 0%, B20%, and B 100% were 142.3 ppm, 41.25 ppm, and 129.31 ppm, respectively. However, the results show that CO emissions at low and high speeds are essentially unresponsive to changes in the mixture composition, which is contrary to observations at medium speeds (between 1500 and 2500 rpm). Blend B20% produced the lowest CO emissions due to its mixing characteristics. This blend produced a better air-fuel mixture with more oxygen due to the lower proportion of oleic acid, methyl ester biofuel. The reduction in CO emissions was not as dramatic as for B20% blend because increasing the biofuel content affects the mixing characteristics and the ability to form a good air-fuel mixture.

Carbon dioxide release

The experimentally determined and numerically expected cycle averages of carbon dioxide (CO_2) emissions are shown in Figure 8b, with values expressed in parts per million (ppm) for the speed range from 800 rpm to 3500 rpm. These results show a good agreement between the numerical results and the experimental results. In the tested engine speed range, the results show low CO_2 emissions for all blends containing biofuel, corresponding to cases B20%, B 40%, B 60%, B 80% and B 100%. The percentage of biofuel made from methyl oleate (ranging from 20% to 100% by volume) has no significant effect on the amount of CO_2 released in the engine exhaust. Although the B20% blend has a slight difference in the CO_2 concentration in the exhaust from the other cases (the difference is less than 1%), the B20% blend produces the lowest CO_2 emissions at all engine speeds. For example, the CO_2 emissions for scenarios B 0%, B20%, and B 100% are 126717 ppm, 109604 ppm, and 110174 ppm, respectively. The oxidative nature of methyl oleate biofuel, where more oxygen is available for combustion, may be the reason for the lower CO_2 emissions. Since biofuels are produced from methyl oleate through photosynthesis, the CO_2 emissions in this scenario are beneficial as they can be considered as carbon credits.

Unburned hydrocarbons releases

Since unburned hydrocarbon emissions are a sign of incomplete fuel combustion, Figure 9a shows the average HC (hydrocarbons) emissions (expressed in ppm) over the speed range of 800 rpm to 3500 rpm [36]. The data in Figure 9a show an increase in HC emissions as the speed increases from 800 to 2000 rpm, where the HC emissions

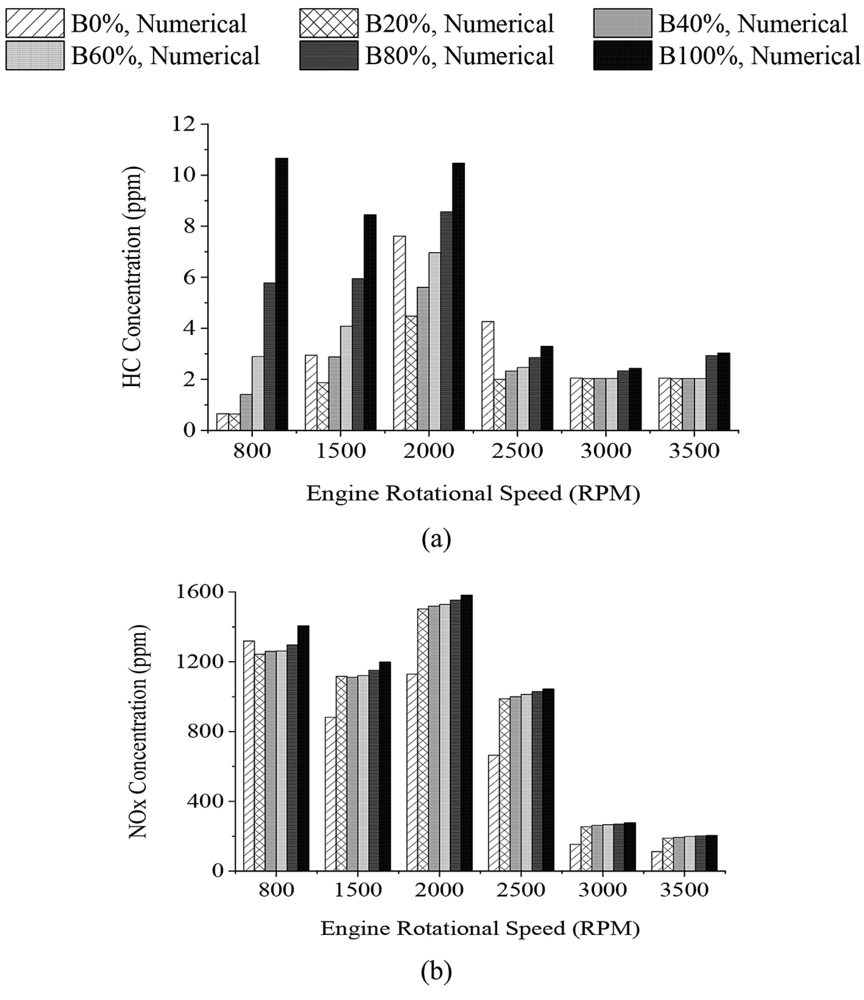

Figure 9. Effect of diesel-OAME blend on cycle average (a) HC and (b) NO_x emissions

peak. HC emissions decrease significantly when the speed increases from 2000 to 3500 rpm. In addition, the results show the sensitivity of HC emissions to fuel composition.

The blend containing 20% B has the lowest HC emissions among all the fuels examined at all speeds. This is because increasing the amount of methyl oleate biofuel in the blend results in higher HC emissions. However, it is important to remember that the HC emissions of pure diesel fuel are always higher than those in the B20% scenario. For example, unburned hydrocarbon emissions were 7.53 ppm, 4.48 ppm, and 10.39 ppm for the B0%, B20%, and B100% cases, respectively. As mentioned in the CO_2 emissions discussion, the oxidizing nature of the blend is responsible for the lower hydrocarbon formation when the B20% blend is used. Higher concentrations of biofuel blends containing methyl oleate do not result in the same low hydrocarbon emissions, likely due to their high viscosity, which is not conducive to optimal injector performance.

Nitrogen oxides releases

Figure 9b shows the cycle averages of nitrogen oxide (NO_x) emissions (numerically predicted and expressed in parts per million (ppm)) over the speed range of 800 rpm to 3500 rpm. These results indicate that the engine produces less NOx in the exhaust at faster speeds. For example, pure diesel fuel has NO_x emissions of 1324.32 ppm and 106.635 ppm at 800 rpm and 3500 rpm, respectively. In addition, the blend containing biofuel and methyl oleate produces more NO_x in the engine exhaust compared to pure diesel. Therefore, if the amount of biofuel containing methyl oleate in the blend increases from 20% to 100%, the NO_x emissions increase by 5.25%. This observation is due to the fact that as the proportion of biofuel containing methyl oleate increases, the oxygen content of the fuel increases, and therefore, more NO_x is emitted. It is important to note that the biofuel produced contains amines, which means that the combustion of these amines in the combustion chamber of the engine cylinder will undoubtedly produce more NOx. Another explanation could be that during the biofuel production process, some of the vitamins bound to nitrogen may have entered the produced biofuel and were not completely separated. When such limited nitrogen is present, the amount of nitrogen oxides produced increases.

CONCLUSIONS

This study investigated the viability of using leftover oil from Tunisia's olive trees in the Sfax region as a substitute for biofuel. Biofuel is made of oleic acid methyl ester, which was extracted using a laboratory-developed transesterification reaction apparatus. Six blends with varying biofuel volume fractions of 0%, 20%, 40%, 60%, 80%, and 100% respectively denoted as B0%, B20%, B40% (blend from biodiesel fuel 40% and fossil diesel fuel 60%), B60% (blend from biodiesel fuel 60% and fossil diesel fuel 40%), B80% (blend from biodiesel fuel 80% and fossil diesel fuel 20%), and B100%, have been created and are being investigated in this study. Next, a single-cylinder, four-stroke engine is used to evaluate the created mixtures. After the engine's performance parameters and exhaust emissions have been experimentally recorded, the outcomes of the 1-D engine simulation program are compared to the numerical data.

The validity of the computational technique has been shown by the difference between the anticipated results and the experimental data, with respect to the brake torque and CO and CO_2 emissions, being less than 10%. In order to better understand the elements influencing the engine's behavior in response to changes in fuel composition, the thermodynamic characteristics of the engine for various diesel-biofuel blends have been examined based on the numerical results. The following conclusions have been taken from the results obtained:

- At low and mid-range engine rotational speeds, the addition of oleic acid methyl ester to the diesel in the final mixture decreased engine brake torque and power; however, at rotational speeds over 2500 rpm, these performance characteristics remain unaffected by changes in fuel composition.
- Because there is not much biofuel in the B20% blend, performance results were about the same as when compared to pure diesel.
- The low fuel calorific value and the growing delay in the combustion start as the blend's content of biofuel rises were blamed for the poor torque that was observed.
- Because there is not much biofuel in the B20% blend, performance results were about the same as when compared to pure diesel. The low fuel calorific value and the growing delay in the combustion start as the blend's

content of biofuel rises were blamed for the poor torque that was observed.

- The engine cycle's pressure-volume diagram has demonstrated the drop in output work that occurs when the pressure drops with a sharp slope with respect to the immediate cylinder volume. The engine has a higher heat loss in the cylinder as well as a high entropy change when it is fueled with a larger percentage of blend-in biofuel, according to the temperature-entropy diagram of the engine cycle.
- As the concentration of biofuel in the mix increased, an increase in fuel consumption of up to 200% was noted at the idle regime of 800 rpm. As the percentage of biofuel in the blend grows, an increase in NO_x emissions has been observed.
- As the fuel composition is changed from the B 0% case to the B 100% case, the fuel combustion is much enhanced, with a 5.58% rise in burn rate.
- The B20% blend had the lowest emissions of carbon monoxide (41.25 ppm) and unburned hydrocarbons (4.48 ppm). The oxygenated nature of the mix and its low viscosity, which is similar to that of a pure diesel and necessary for the injector to operate as best it can to ensure appropriate spray characteristics, are the reasons for the low emissions of HC and CO when using the B20% blend.
- The blend B20%, which is made up of 20% volume fraction of transesterified used olive oil and 80% volume fraction of pure diesel, can be a useful substitute fuel because it allows for reduced pollutant emissions while maintaining engine performance, according to all the results.

REFERENCES

1. Alagumalai, A., Mahian, O., Hollmann, F. and Zhang, W. (2021). Environmentally benign solid catalysts for sustainable biodiesel production: A critical review. Science of the Total Environment, 768, 144856.
2. Al-Aseebee, M.D., Akol, A.M. and Naje, A.S. (2023). Performance evaluation of tractor engine using waste vegetable oil biodiesel for agricultural purpose. Ecological Engineering & Environmental Technology, 24.
3. Moussa, O., Ketata, A., Zied, D., Coelho, P. (2019). In-cylinder aero-thermal simulation of compression ignition engine: Using a layering meshing approach. Journal of Applied Fluid Mechanics, 12(5), 1651–1665.
4. Ketata, A., Driss, Z., Abid, M.S. (2020). Impact of the wastegate opening on radial turbine performance under steady and pulsating flow conditions. Proceedings of the Institution of Mechanical Engineers, Part D: Journal of Automobile Engineering, 234(2–3), 652–668.
5. Ketata, A. and Driss, Z. (2021). New FORTRAN meanline code for investigating the volute to rotor interspace effect on mixed flow turbine performance. Proceedings of the Institution of Mechanical Engineers, Part E: Journal of Process Mechanical Engineering, 235(5), 1511–1521.
6. Bórawski, P., Bełdycka-Bórawska, A., Szymańska, E.J. et al. (2019). Development of renewable energy sources market and biofuels in The European Union. Journal of cleaner production, 228, 467–484.
7. Yan, J. and Lin, T. (2009) Biofuels in asia., Elsevier, 1–10.
8. Al-Aseebee, M.D., Rashid, A.H., Naje, A.S. (2021). Ecofriendly enhancement of engine performance using biofuel palm stearin. Materials Today: Proceedings.
9. Millo, F., Vlachos, T., Piano A. (2021). Physico-chemical and mutagenic analysis of particulate matter emissions from an automotive diesel engine fuelled with fossil and biofuel blends. Fuel, 285, 119092.
10. Al-Aseebee, M.D., Al-Aseebee, M.D.F, Ketata, A., Gomaa, A.E., et al. (2023). Modeling of waste vegetable oil biodiesel for tractor engine utilization. Journal of Ecological Engineering, 24(12).
11. Lin, C.-Y. and Lu, C. (2021). Development perspectives of promising lignocellulose feedstocks for production of advanced generation biofuels: A review. Renewable and Sustainable Energy Reviews, 136, 110445.
12. Al-Aseebee, M.D., Naje, A.S. (2023). The influence of olive oil waste as a biofuel on the exhaust gases of the internal combustion engine. Journal of Ecological Engineering, 24(5).
13. Tomar, M., Dewal, H. Sonthalia, A., Kumar, N. (2021). Optimization of spark-ignition engine characteristics fuelled with oxygenated bio-additive (triacetin) using response surface methodology. Proceedings of the Institution of Mechanical Engineers, Part E: Journal of Process Mechanical Engineering, 235(4), 841–856.
14. Karishma, S.M., Dasore, A., Rajak, U., et al. (2022). Experimental examination of CI engine fueled with various blends of diesel-apricot oil at different engine operating conditions. Materials Today: Proceedings, 49, 307–310.
15. Bhanu Teja, N., Devarajan, Y., Mishra, R., et al., (2021). Detailed analysis on sterculia foetida kernel oil as renewable fuel in compression ignition engine. Biomass Conversion and Biorefinery, 1–12.
16. Pimenta, J.L.C.W., Camargo, M.O., Duarte, R.B. et al. (2021). Deoxygenation of vegetable oils for the production of renewable diesel: Improved aerogel based catalysts. Fuel, 290, 119979.
17. Shrigiri, B.M. (2022). Combustion characteristics of

sugar apple seed (Annona squamosa) oil methyl ester and its blends on compression ignition engine. International Journal of Ambient Energy, 43(1), 4370–4379.
18. Narowska, B.E., Kułażyński, M. and Łukaszewicz M. (2020). Application of activated carbon to obtain biodiesel from vegetable oils. Catalysts, 10(9), 1049.
19. Qiu, F., Li, Y., Yang, D. et al. (2011). Biodiesel production from mixed soybean oil and rapeseed oil. Applied Energy, 88(6), 2050–2055.
20. Kumar, A., Tripathi, R.K., Ranjan, S. and Hasan, A.S. (2020). Performance and emission analysis of microalgae biofuel-diesel blends in internal combustion engine. Int. J. Eng. Res. Technol, 9(4), 378–392.
21. Karikalan, L. and Chandrasekaran, M. (2015). Karanja oil biodiesel: a potential substitution for diesel fuel in diesel engine without alteration. Arpn Journal Of Engineering And Applied Sciences, 10.
22. Salaheldeen, M., Aroua, M.K., Mariod, A.A. et al. (2015). Physicochemical characterization and thermal behavior of biodiesel and biodiesel–diesel blends derived from crude Moringa peregrina seed oil. Energy Conversion and Management, 92, 535–542.
23. Alaseebee, M.D.F., Ketata, A., Hasan, H.A.R., Moussa, O., Driss, Z., Abid, M.S., Naje, A.S., Hussain, T.H. (2024). Numerical and experimental analyses for performance and emissions assessment of a four-stroke engine powered by oleic acid methyl ester biofuel made from waste frying oil. Global NEST Journal, 26(8).
24. Baiju, B., Naik, M. and Das, L. (2009). A comparative evaluation of compression ignition engine characteristics using methyl and ethyl esters of Karanja oil. Renewable energy, 34(6), 1616–1621.
25. Hou, J., Zhang, H., Yanet, X., et al. (2021). Experimental study on dynamic injection behaviors of biodiesel and its blends in a common-rail injection system. Proceedings of the Institution of Mechanical Engineers, Part C: Journal of Mechanical Engineering Science, 235(1), 179–189.
26. Li, C., Zhang, Q. and Hu X., et al., (2021). Effect of rGO@ Fe_3O_4 on the tribological behavior of biodiesel soot-contaminated polyalphaolefin. Proceedings of the Institution of Mechanical Engineers, Part J: Journal of Engineering Tribology, 235(3), 668–676.
27. Chourasia, S.K., Lakdawala, A.M., Patel, R.N. (2021). The examination, evaluation and comparison of corrosion effect on different metal surface by various crops based biodiesel. Proceedings of the Institution of Mechanical Engineers, Part C: Journal of Mechanical Engineering Science, 235(19), 4409–4424.
28. Yi, B., Song, L., Li F., et al. (2019). Experimental study of the effect of n-butanol additive on spray characteristics of biodiesel in a high-pressure common-rail injection system. Proceedings of the Institution of Mechanical Engineers, Part A: Journal of Power and Energy, 233(2), 211–220.
29. Abed, K., Gad, M.S., El Morsi, A.K. et al. (2019). Effect of biodiesel fuels on diesel engine emissions. Egyptian journal of petroleum, 28(2), 183–188.
30. Tarabet, L., Loubar, K., Lounici, M.S., et al. (2012). Eucalyptus biodiesel as an alternative to diesel fuel: preparation and tests on DI diesel engine. BioMed Research International, 2012(1), 235485.
31. Kulkarni, M.G. and Dalai, A.K. (2006). Waste cooking oil an economical source for biodiesel: a review. Industrial & engineering chemistry research, 45(9), 2901–2913.
32. Ketata, A. and Driss, Z. (2021). Characterization of double-entry turbine coupled with gasoline engine under in-and out-phase admission. Energy, 236, 121447.
33. Ketata, A., Driss, Z., Abid, M.S. (2019). 1D gas dynamic code for performance prediction of one turbocharger radial turbine with different finite difference schemes. Mechanics & Industry, 20(6), 627.
34. Ketata, A. and Driss, Z. (2022). A methodology for loss and performance assessment of a variable geometry turbocharger turbine through a new meanline FORTRAN program. Engineering Computations, 39(4), 1597–1620.
35. Bari, S. (2014). Performance, combustion and emission tests of a metro-bus running on biodiesel-ULSD blended (B20) fuel. Applied Energy, 124, 35–43.
36. Heywood, J.B. (2018). Internal combustion engine fundamentals. McGraw-Hill Education.